JOURNAL OF SPACECRAFT AND ROCKETS
Vol. 37, No. 5, September–October 2000

Study of Quartz Surface Catalycity in Dissociated Carbon Dioxide Subsonic Flows

Anatoly F. Kolesnikov,* Ivan S. Pershin,† Sergey A. Vasil'evskii,‡ and Mikhail I. Yakushin§
Russian Academy of Sciences, 117526, Moscow, Russia

The stagnation point heat transfer from subsonic dissociated carbon dioxide flows to quartz and cooled metallic surfaces has been measured by calorimetry and studied numerically. The aerothermal tests were performed using the 100-kW IPG-4 inductive plasmatron at 10^4 Pa pressure in the enthalpy range 14.4–38.5 MJ/kg. The numerical simulation included the computations of the carbon dioxide inductively coupled plasma torch, of the subsonic reacting flows around a cylindrical model, and in a nonequilibrium boundary layer. The model of catalysis based on the Eley–Rideal mechanism, in which adsorption of oxygen atoms predominates over other species adsorption, is proved to be sufficient to explain the heat transfer data. Silver is found to be the best catalyst and molybdenum a poor one. The efficiencies of the catalytic recombination reactions $O + O \rightarrow O_2$ and $CO + O \rightarrow CO_2$ on quartz and silica-based thermal protection surface have been determined and combined in the surface temperature range 390–1670 K by comparing the experimental and numerical heat transfer data. The catalytic efficiencies of quartz- and silica-based surfaces in dissociated carbon dioxide appeared to be quite similar to the ones obtained in dissociated pure oxygen. The maximum of an average catalytic efficiency for both reactions on silica has been revealed at the surface temperature 1470 K ($\gamma_w \approx 6 \times 10^{-3}$). Adsorption and desorption of oxygen atoms play the key roles in catalysis on silica-based surfaces in dissociated carbon dioxide flows. For the prediction of the aeroheating silica-based thermal-protection surfaces during entry into the Martian atmosphere, an approximation of the catalytic efficiency as a function of surface temperature in the range 390–1670 K is given.

Nomenclature

b = thickness of the heat reception wall of a quartz calorimeter, mm
C = mass fraction
D = diameter of the plasmatron discharge channel, mm
F = frequency of rf generator, MHz
f = dimensionless stream function
G = mass flow rate through discharge channel, g/s
h = gas enthalpy, MJ/kg
I = dimensionless mass diffusion flux
J = mass diffusion flux, kg/(m^2 s)
K_w = catalytic recombination rate constant, m/s
k = Boltzmann constant
M = Mach number
m = dimensionless molecular weight of the gas mixture
m_i = molecular weight of species i, kg
N_{ap} = anode power of the rf generator, kW
N_{pl} = power input in plasma, kW
Pr = Prandtl number
p = pressure, Pa
q = stagnation point heat flux, W/cm^2
q_c = heat loss density measured by water-cooled calorimeter, W/cm^2
Re = Reynolds number
R_m = model radius, m
r = normal cylindrical coordinate related to the model surface, m
S = site for the surface-adhered atom
Sc = Schmidt number
T = temperature, K
U = longitudinal velocity component in the cylindrical coordinate system, m/s
u = dimensionless velocity gradient
V = flow velocity along central line, m/s
y^0 = longitudinal cylindrical coordinate related to the model surface, m
α = dimensionless external flow vorticity
γ = surface catalytic efficiency
Δ = dimensionless boundary-layer thickness
δ = boundary-layer thickness, m
ε_{th} = surface total hemispherical emissivity
ε_λ = quartz spectral emissivity
η = dimensionless boundary-layer variable
μ = viscosity, N · s/m^2
ρ = density, kg/m^3
σ = Stefan–Boltzmann constant
τ_{VT} = Landau–Teller relaxation time, s
φ = angle of flow swirling

Subscripts

e = boundary-layer outer edge
i = mixture species i
s = freestream conditions in plasmatron jet
w = wall

Introduction

SURFACE catalysis affects essentially the vehicle surface heating during a hypersonic entry into the Martian rarefied atmosphere.[1–4] At the trajectory peak-heating points, according to calculations of Refs. 1–4, the stagnation point heat fluxes to the Mars Pathfinder aeroshell, MARSNET, and Mars probe shields are almost three times greater in the case of a fully catalytic surface in respect to reactions $CO + O \rightarrow CO_2$ and $O + O \rightarrow O_2$ than in the noncatalytic heating case. Therefore, the search and application of the low catalytic thermal-protection materials (TPM) for the Mars missions look quite promising and profitable in the scope of decreasing mass of the thermal-protection system (TPS).

When this study was initiated, there existed some previous data on the catalytic recombination of oxygen on silica-based materials[5–7]

Presented as Paper 98-2847 at the AIAA/ASME 7th Joint Thermophysics and Heat Transfer Conference, Albuquerque, NM, 15–18 June 1998; received 3 December 1999; revision received 22 May 2000; accepted for publication 23 May 2000.

*Senior Scientist, Institute for Problems in Mechanics, Plasma Laboratory, Prospect Vernadskogo 101/1. Member AIAA.
†Research and Development Engineer, Institute for Problems in Mechanics, Plasma Laboratory, Prospect Vernadskogo 101/1.
‡Senior Scientist, Institute for Problems in Mechanics, Plasma Laboratory, Prospect Vernadskogo 101/1.
§Head of Plasma Laboratory, Institute for Problems in Mechanics, Prospect Vernadskogo 101/1.

in contrast to lack of any data on the catalytic recombination of carbon monoxide on silica at high temperatures. The present paper deals with heat transfer in dissociated carbon dioxide mixture and with numerical rebuilding joint contribution of the two mentioned catalytic reactions to surface heating, though without actual sharing between O-atom recombination to form O_2 and CO + O recombination to form CO_2.

The first known heat transfer tests with high-enthalpy carbon dioxide gas flows were conducted using the 100-kW IPG-4 inductive plasmatron at the stagnation pressure 10^4 Pa in the enthalpy range 11.4–38.5 MJ/kg (Refs. 8 and 9). In subsonic dissociated unpolluted carbon dioxide gas flows the stagnation point heat flux to a 50-mm-diam cylindrical model with a flat face (so-called euro-model) covered with a black glassy Si-based coating, used long before for the Buran thermal-protection tile, decreased a factor two in comparison with a calculated heat flux to a fully catalytic surface. The first data for the catalytic efficiencies of the heterogeneous reactions $CO + O \rightarrow CO_2$ and $O + O \rightarrow O_2$ on the Buran tile coating ($T_w = 1470$–1670 K), on two coatings of the carbon–carbon TPM ($T_w = 1420$–1840 K), and on the quartz surface ($T_w = 390$–1470 K) were extracted by means of comparing the measured and calculated stagnation point heat transfer rates.[8,9]

The objectives of this work are the further development of the method to predict catalycity of the thermal-protection surfaces for the Martian entry heating conditions and the determination of the average catalytic efficiency of quartz related to catalytic reactions $O + O \rightarrow O_2$ and $CO + O \rightarrow CO_2$ at high surface temperatures. The logic of the surface catalycity determination is based on the contribution of catalytic recombination of O atoms and CO molecules in surface heating, which can be extracted numerically from the measured stagnation point heat flux. In general, the methodology to determine catalytic properties of the Buran TPM related to the atomic nitrogen and oxygen recombination in subsonic aerothermal tests was developed in the 1980s.[10,11] There were two main reasons to choose quartz for the present research. First, quartz catalycity in respect to N and O-atoms recombination is close to the catalycity of the Si-based materials used for the space shuttle[5–7] and Buran.[10,11] Second, quartz differs from other materials by the high stability of surface properties in oxidizing environment and can be used as a reference material.

In this paper, the data on the average efficiency of catalytic reactions $O + O \rightarrow O_2$ and $CO + O \rightarrow CO_2$ on the quartz surface in the wide temperature range $T_w = 470$–1470 K at the pressure 10^4 Pa are obtained and combined with data of Ref. 8. The pressure was specified as an intermediate one between stagnation pressures at the peak-heating points of the Mars Pathfinder[2] and Mars Probe[12] entry trajectories. Our comparative study of the catalytic heating in high-enthalpy subsonic pure oxygen and carbon dioxide flows has confirmed that an average catalytic efficiency for reactions $O + O \rightarrow O_2$ and $CO + O \rightarrow CO_2$ on quartz surface can be used.[13] The present paper reports that catalytic efficiencies of silica-based surfaces in dissociated carbon dioxide are similar to previous results[6,7] for the catalytic recombination of atomic oxygen. An experimental investigation of the relative importance of these reactions on quartz in the temperature range 292–623 K has been performed recently using a diffusion tube side-arm reactor together with two-photon laser-induced fluorescence for both O and CO species detection.[14] Our results are confirmed by the finding in Ref. 14 that O-atom recombination is the dominant surface reaction on quartz in mixtures of O and CO. An analysis of Ref. 15 based on the present data has predicted a factor two for the reduction of the maximum fully catalytic heating the Mars Probe surface if a silica-based material is applied.

Philosophy of the Method

The general philosophy of the TPM catalycity prediction on the basis of subsonic aerothermal tests developed in Refs. 8–11 consists of the tight connection of the TPM catalycity determination with quantitative heat transfer simulation for the atmospheric entry conditions. In fact, the method reveals a correct way to extrapolate from ground test to flight based on the concept of a local simulation of the stagnation point heat transfer.[11,15,16] The methodology includes the following essential parts: 1) performance and optimization of the subsonic high-enthalpy test with different gases (carbon dioxide, oxygen, nitrogen, air), 2) steady-state heat transfer tests in the stagnation point configuration, 3) characterization of the plasmas and reacting gas flows, 4) demonstration of the catalysis heating effects, 5) search and application of materials with standard catalytic properties, 6) computational fluid dynamics (CFD) modeling inductively coupled plasma torches and reacting gas flows around a model for test conditions, 7) numerical rebuilding the freestream enthalpy and flowfield around a model, 8) model of the surface catalysis, 9) numerical design of the heat flux charts for test conditions and an analysis of the heat transfer data, 10) extrapolation from ground test to atmospheric entry conditions, and 11) analysis of uncertainties. All of these indispensable parts of the methodology are considered or at least touched on in the present paper.

Subsonic Tests

The aerothermal tests were performed using the 100-kW IPG-4 inductive plasmatron[8,9,17] located at the Institute for Problems in Mechanics of the Russian Academy of Sciences. The exceptional purity of high-enthalpy gas flows, excellent reproducibility and high stability of freestream conditions, and long duration of plasmatron operation are provided by means of the inductive heating. The main plasmatron parameters are as follows: $N_{ap} = 20$–75 kW, $F = 1.76$ MHz, $D = 80$ mm, and $G = 1.5$–3 g/s. The remarkable aerothermal capabilities of the IPG-4 plasmatron for the duplication of the stagnation point heat flux to the Mars Probe vehicle have been analyzed and validated in Refs. 15 and 18.

For the purpose of the present research, the stable subsonic flows of dissociated carbon dioxide gas were produced at the static pressure 10^4 Pa and $G = 1.8$ g/s in the enthalpy range 14.4–38.5 MJ/kg. The specified pressure was chosen between the stagnation pressures for the Mars Pathfinder aeroshell (1.35×10^4 Pa) (Ref. 2) and the Mars Probe shield (7×10^3 Pa) (Ref. 12) at the trajectory peak-heating points. In fact, the realized enthalpy range was much wider then the total enthalpy ranges for the Mars Pathfinder and Mars Probe entry trajectories.

The 50-mm-diam water-cooled copper model (Fig. 1) was used in the experimental study of the stagnation point heat transfer to silver, copper, molybdenum, and quartz surfaces. The distance between the model and the discharge channel exit section was 60 mm. In the stagnation point configuration, the following optimum subsonic test conditions were realized: 1) axially symmetric flow past a model, 2) flow perturbations induced by the model not reaching the discharge channel, 3) high stability of the freestream conditions, 4) uniform heat loading on the heat probe (calorimeter) surface, and 5) good reproducibility of stagnation point heat transfer.

The variation of the freestream conditions and stationary heat transfer to the model surface at constant pressure and gas flow rate were provided by the control of the anode power N_{ap} supplied to the inductor. With N_{ap} increasing, the power input in plasma increases, as well as flow enthalpy, velocity, stagnation point heat flux, and quartz surface temperature.

For the stagnation point heat flux measurements, the water flow steady-state calorimeters made of copper monolith, monocrystalline molybdenum, and quartz of high chemical purity were applied along with the calorimeter with silver front face. The heat reception surfaces of the calorimeters were polished. To vary quartz surface temperature at a selected plasmatron operating regime, the quartz probes

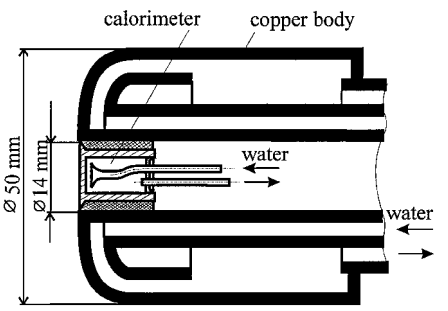

Fig. 1 Test model schematic.

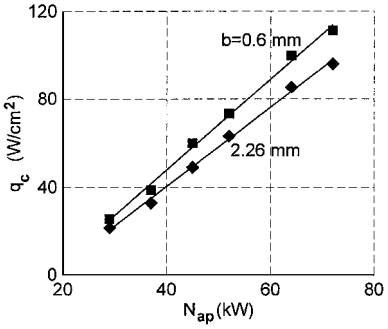

Fig. 2 Heat loss densities into quartz calorimeters vs anode power.

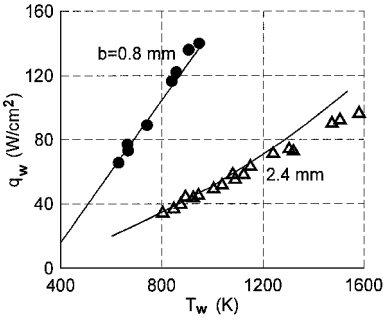

Fig. 3 Stagnation point heat fluxes to quartz calorimeters vs surface temperature.

with the different thickness of the heat reception wall $b = 0.63$, 1.43, and 2.26 mm were used.

The water temperature in the calorimeter was measured with thermocouples with accuracy 0.1°C. The water flow rate was measured with the float rotameter with an error ±1.5%. The measurement accuracy of the stagnation point heat flux to the cooled surface ($T_w \approx 300$ K) was ±5%.

The stagnation point heat flux to the high-temperature quartz surface was determined by

$$q_w = \varepsilon_{\text{th}} \sigma T_w^4 + q_c \tag{1}$$

The surface temperature T_w was obtained by the solution of the one-dimensional heat transfer problem in the heat reception quartz wall taking into account the well-documented temperature dependence for the quartz thermal conductivity.[19] The literature data[20,21] on the total quartz surface emissivity for the different wall thickness were used to determine the heat flux q_w. The measurement accuracy of the heat flux to quartz surface was ±7%. Figure 2 presents the results of measurements of the heat loss density q_c at different values of the power N_{ap} for the two quartz probes.

Figure 3 shows the calculated dependencies $q_w(T_w)$ for the quartz probes with thickness $b = 0.8$ and 2.4 mm in comparison with the calibration data obtained in high-enthalpy nitrogen flows. In the calibration tests, quartz surface temperature was measured with the thermovision system AGA-780 at the effective wave length $\lambda = 5\mu$m, where the quartz spectral emissivity ε_λ did not depend on surface temperature: $\varepsilon_\lambda = 0.98$. With the power variation in the range $N_{\text{ap}} = 29$–72 kW, the ranges of the quartz surface temperature and of the heat flux to the quartz surface were realized as follows: $T_w = 390$–1470 K and $q_w = 26$–111 W/cm^2.

The characterization of high-enthalpy carbon dioxide subsonic flows included measurements of the stagnation point heat flux to a silver surface, which turned out to be the best catalyst in dissociated carbon dioxide flows, and the velocity head at the jet axis at 60 mm distance from the discharge channel exit. The velocity head measurements were performed with the copper water-cooled pitot tube with the same geometry as the model used for the heat flux measurements.

CFD Modeling

The numerical simulation of subsonic high-enthalpy flows and heat transfer for the plasmatron tests conditions is an essential part of the freestream conditions rebuilding and surface catalycity determination.[9–11,22] The CFD modeling includes the three problems as follows: 1) the equilibrium inductively coupled plasma flow in a cylindrical discharge channel, 2) the subsonic laminar reacting jet flow past a cylindrical model, and 3) the nonequilibrium boundary layer at a model stagnation point.

The first problem dealing with thermal plasmas chemistry and material processing is a well-known one in the literature.[23] Some computations of inductively coupled air plasma focused on applications for reentry issues were published in Refs. 22 and 24. In the present paper, the first problem has been solved on the basis of the full Navier–Stokes equations coupled with the simplified Maxwell equations for rf electromagnetic field.[24] The two-dimensional Navier–Stokes equations were written for the total enthalpy and three velocity components including the tangential component due to the flow swirling. The simplified quasi-one-dimensional Maxwell equations were used to calculate the complex amplitude of the electric field tangential component generating vortical electric currents in CO_2 plasma in the discharge channel. The input parameters for the problem were the torch geometry, the inductor electric current frequency F, the gas flow rate G, the static pressure p, the power input in plasma N_{pl}, and the angle of gas swirling at the inlet section φ.

The finite difference analogies of the Navier–Stokes equations were written for control volumes using the staggered grid. The obtained equations were solved by a method similar to Patankar and Spalding SIMPLE method (see Ref. 25). The final system of linear algebraic equations was solved by the modified method of incomplete factorization. The simplified equation for the complex amplitude of the electric field tangential component was solved in every cross section by an effective technique based on the Thomas algorithm.

The recent code-to-code validation for the IPG-4 test case with an argon inductively coupled plasma[26] has shown a rather good agreement between one-dimensional electric field approach[22,24] and complete two-dimensional formulation for the plasma-induced electric field inside the discharge channel and in the space beyond the torch itself.[27] The plasma flow patterns and temperature fields in the whole discharge channel, including the plasmatron exit section, obtained independently by the two methods were found to be consistent.[26]

Particular attention was paid to calculations of the plasma transport properties: thermal conductivity and electrical conductivity. These transport coefficients were calculated in advance as the functions of enthalpy and pressure taking into account higher approximation by Sonine polynomials (the third one) for the distribution functions according to requirements of Ref. 28 for highly ionized gases. The modified procedure of the Chapman–Enskog method (developed in Ref. 29) was used to reduce sufficiently the order of determinants calculating the thermal conductivity and electrical conductivity of multicomponent ionized carbon dioxide gas mixture.

The calculated isolines of the stream function and isotherms of carbon dioxide plasma in the plasma torch are shown in Fig. 4 for $p = 10^4$ Pa, $G = 1.8$ g/s, $N_{\text{pl}} = 25$ kW, and $\varphi = 45$ deg. The complicated pattern of the inductively coupled plasma flow is formed

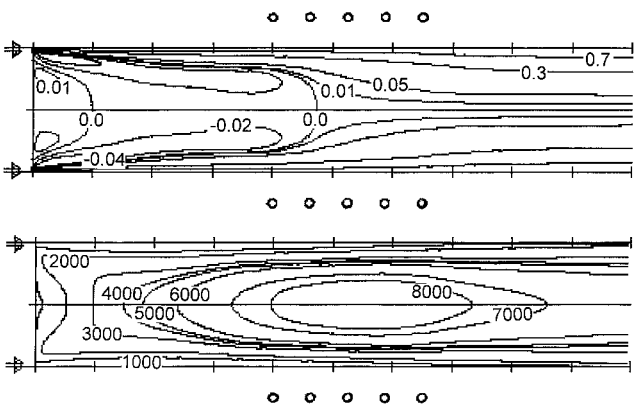

Fig. 4 Isolines of dimensionless stream function and isotherms in plasma torch at N_{pl} = 25 kW.

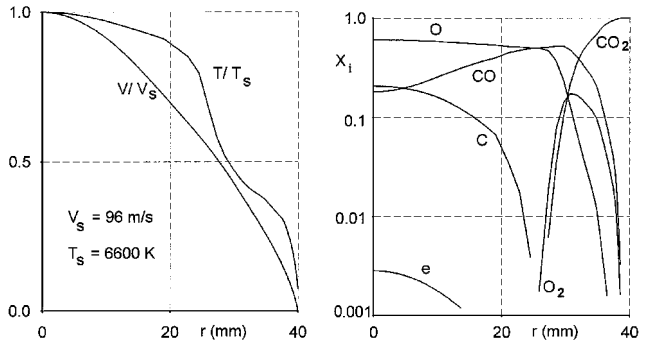

Fig. 5 Radial profiles of dimensionless velocity, temperature, and species molar fractions at the plasmatron exit at N_{pl} = 25 kW.

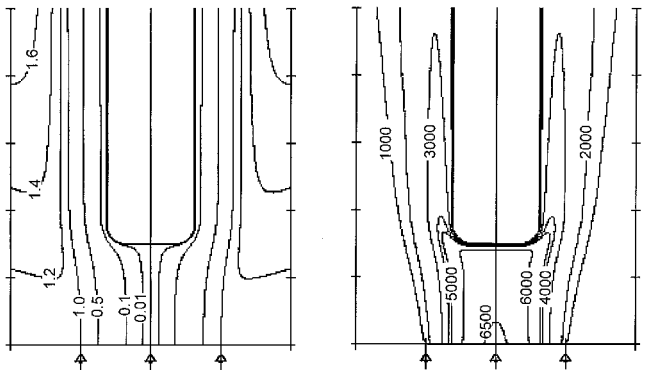

Fig. 6 Flow and temperature fields around the test model at N_{pl} = 25 kW.

due to the interaction of a swirling gas flow with Joule's heating and magnetic pressure. The calculated equilibrium plasma flow profiles at the torch exit (see Fig. 5) are the inflow boundary conditions for the second mentioned CFD problem.

In Fig. 5 one can see quite specific features of the subsonic flow at the torch exit: the high-enthalpy, low-velocity flow implies CO molecules, O atoms, C atoms, and a weak trace of electrons in the jet core. For this flow regime, the Landau–Teller relaxation time for CO molecules $\tau_{VT} \sim 2 \times 10^{-5}$ s, so that the relaxation zone length ($\sim 2 \times 10^{-3}$ m) is much shorter than the distance from the torch exit to the model (6×10^{-2} m). Taking this into account, we assume that the subsonic jet is under conditions of local thermodynamic equilibrium (LTE), though one could expect some displacement from LTE in the mixing layer and strong nonequilibrium effects in the boundary layer near a model. The reason for this approach is the use of a numerical solution for an equilibrium jet flow past a model only as an external solution for the nonequilibrium boundary-layer problem.

Full two-dimensional Navier–Stokes equations for enthalpy and two velocity components have been used to simulate the laminar hyposonic ($M \ll 1$) high-enthalpy carbon dioxide flow over the model under LTE (tangential swirling and ionization were not essential factors in the heat transfer here). The same numerical method[25] was used to solve the governing equations. Computations were performed for the cold wall case ($T_w = 300$ K). Surface catalycity was not a factor in this problem.

Figure 6 shows the central parts of the calculated flow and temperature fields around a model and confirms (qualitatively) the LTE approach in the core of the subsonic jet. In fact, we observe the large isothermal and isobaric zone between the plasma torch exit and a model, the favorable conditions for the fast relaxation.

To simulate heat and mass transfer through a nonequilibrium boundary layer to the stagnation point, the equations of boundary layer with finite thickness[8–11] have been used. Because weak ionization in the freestream did not affect heat transfer to a model at the considered test conditions, the following physical model of the nonequilibrium boundary layer was assumed: 1) the gas is a five-species mixture of the molecules and atoms CO_2, O_2, CO, C, and O; 2) molecules vibrations are in equilibrium excitation and chemical kinetics is one temperature; and 3) the following reactions proceed in the mixture:

$$CO_2 + M \leftrightarrow CO + O + M, \qquad O_2 + M \leftrightarrow O + O + M$$

$$CO + M \leftrightarrow C + O + M, \qquad CO + O \leftrightarrow C + O_2$$

$$CO_2 + O \leftrightarrow CO + O_2, \qquad M = CO_2, O_2, CO, C, O$$

The data on the rate constants for the gas-phase reactions were taken from Ref. 30.

The simple scheme of the surface catalysis was assumed as follows: 1) The adsorption of O atoms predominates over other species adsorption. 2) The adsorption of O atoms and desorption of products from the surface are fast reactions. 3) The heterogeneous reactions $O + O \rightarrow O_2$ and $CO + O \rightarrow CO_2$ follow the simple model of Eley–Rideal mechanism (see Ref. 31) of the O and CO recombination

$$O + S \rightarrow O\_S, \qquad O + O\_S \rightarrow O_2 + S$$

$$CO + O\_S \rightarrow CO_2 + S$$

where S is a surface site and O_S is the surface-adhered O-atom. 4) The heterogeneous reaction $C + 2O \rightarrow CO_2$ is a two-step reaction, which follows the simple model of Langmuir–Hinshelwood (see Ref. 31) with the fast second step

$$C + O\_S \rightarrow CO\_S, \qquad CO\_S + O\_S \rightarrow CO_2 + 2S$$

where CO_S is the surface-adhered CO-molecule. 5) All efficiencies of earlier catalytic reactions γ_{wO}, γ_{wCO}, and γ_{wC} are equal to some average value γ_w.

In this way we have introduced the average efficiency of recombination γ_w. The reason for this approach links with the fact that actually there is only the measured parameter q_w, which allows to extract numerically only the joint contribution of catalytic reactions to surface heating and, thus, to determine the effective surface catalycity. Our comparative analysis of the heat transfer data obtained in high-enthalpy subsonic pure oxygen and carbon dioxide flows using the IPG-4 facility has confirmed that the use of an average catalytic efficiency for reactions $O + O \rightarrow O_2$ and $CO + O \rightarrow CO_2$ on quartz surface is possible.[13]

This scheme of surface catalysis leads to the first-order surface recombination of CO molecules and O and C atoms. Respectively, boundary conditions at the surface for the mass fractions of CO molecules and O and C atoms are written as follows:

$$-J_{CO} = \rho K_{wCO} C_{CO}, \qquad -J_O = \rho K_{wO} C_O \tag{2}$$

$$-J_C = \rho K_{wC} C_C \tag{3}$$

where

$$K_{wi} = [2\gamma_w/(2 - \gamma_w)]\sqrt{kT_w/2\pi m_i} \tag{4}$$

The first two conditions (2) are close to those used in Ref. 2. Practically, during the entry into the Martian atmosphere, the catalytic recombination of C atoms does not play any role in the heat transfer to a vehicle.[2] However, for the actual plasmatron test conditions, the heterogeneous reaction $C + 2O \rightarrow CO_2$ is included in the model of surface catalysis to provide total energy balance for a fully catalytic wall ($\gamma_w = 1$) in the entire enthalpy range. At the enthalpies above 35 MJ/kg, atomic carbon in freestream contains some noticeable amount of energy of the C-atoms formation. This energy remains in latent form and is not released on the surface in the case $\gamma_{wO} = \gamma_{wCO} = 1$ and $\gamma_{wC} = 0$. That means, in this case, the surface being fully catalytic at moderate enthalpies turns out to be partially catalytic at high enthalpies. As a result, the numerical rebuilding of the freestream enthalpy from the measured heat flux to a cold fully catalytic wall is correct if $\gamma_{wO} = \gamma_{wCO} = \gamma_{wC} = 1$. In addition, it is

necessary to use the single boundary condition of the O or C atoms balance on the surface:

$$J_{O_2} + \left(2m_O/m_{CO_2}\right)J_{CO_2} + (m_O/m_{CO})J_{CO} + J_O = 0 \quad (5)$$

$$\left(m_C/m_{CO_2}\right)J_{CO_2} + (m_C/m_{CO})J_{CO} + J_C = 0 \quad (6)$$

The governing equations of the one-dimensional boundary layer with finite thickness are given as follows:

$$(\ell u'_\eta)_\eta + f u'_\eta - \frac{1}{2}u^2 + \frac{1}{2}\frac{1+\alpha_e}{\rho} = 0 \quad (7)$$

$$f'_\eta = u \quad (8)$$

$$\left(\frac{\ell}{Pr}h'_\eta\right)'_\eta + f h'_\eta - \left[\frac{\ell}{Pr}\sum_{i=1}^{5}\left(h_i - h_i^*\right)(Le_i - 1)C'_{i\eta}\right]_\eta = 0 \quad (9)$$

$$\left(\frac{\ell}{Sc_i}C'_{i\eta}\right)'_\eta + f C'_{i\eta} + \dot{w}_i = 0 \quad (10)$$

$$\frac{1}{\rho} = \frac{T}{m}, \qquad \sum_{i=1}^{5} C_i = 1, \qquad h = \sum_{i=1}^{5} h_i \quad (11)$$

where

$$\ell = \frac{\mu\rho}{\eta_e^2}, \qquad \eta_e = \frac{\Delta\sqrt{2Reu_{1e}}}{\chi}, \qquad Re = \frac{\rho_s V_s R_m}{\mu_e}$$

$$y = \frac{y^0}{R_m}, \qquad \Delta = \frac{\delta}{R_m}, \qquad u = \frac{u_1}{u_{1e}}, \qquad u_1 = \frac{R_m}{V_s}\frac{\partial U}{\partial r}$$

$$\alpha_e = -\frac{V_e}{V_s}\frac{R_m}{u_{1e}^2}\left(\frac{\partial u_1}{\partial y^0}\right)_e, \qquad \chi = \int_0^1 \frac{\mathrm{d}\eta}{\rho}$$

The boundary conditions at the outer edge ($\eta = 1$) and the model surface ($\eta = 0$) are written as follows:

$$\eta = 1: \quad u = h = 1, \qquad C_i = C_{ie} \quad (12)$$

$$\eta = 0: \quad u = f = 0, \qquad T = T_w \quad (13)$$

$$-I_O = (K_{wO}/V_s)\rho\kappa C_O, \qquad -I_{CO} = (K_{wCO}/V_s)\rho\kappa C_{CO} \quad (14)$$

$$-I_C = (K_{wC}/V_s)\kappa\rho C_C$$

$$-I_{CO_2} = \left(m_{CO_2}/m_{CO}\right)I_{CO} + \left(m_{CO_2}/m_C\right)I_C \quad (15)$$

where

$$I_i = -(\ell/Sc_i)C'_{i\eta}, \qquad \kappa = (1/\eta_e)\sqrt{Re/2u_{1e}}$$

The governing equations (7–11) account for the finite boundary-layer thickness and flow vorticity at the outer edge of the boundary layer by means of three dimensionless parameters, Δ, u_{1e}, and α_e, and provide accurate computations of the stagnation point heat flux. These dimensionless parameters were obtained from the numerical solution of the full Navier–Stokes equations for the dissociated carbon dioxide subsonic jet flow over a test model under LTE (see Fig. 6). At constant gas flow rate, these parameters actually depended slightly on pressure and power input in plasma. The solutions of the Navier–Stokes equations and boundary-layer equations were matched at the distance from surface δ (finite boundary-layer thickness), where the profile $u_1(y)$ has the only inflection point. The finite difference scheme of the fourth order of approximation was used for the numerical solution of the one-dimensional boundary-layer problem.

Results and Discussion

In performed cold wall tests ($T_w = 300$ K) maximum heat fluxes were registered on the silver surface and minimum ones on the molybdenum surface. Heat fluxes to copper were found to be a little less than heat fluxes to silver. These results allow the arranging the metals along the catalycity scale: Ag > Cu > Mo. Strictly speaking, the catalycity scale is arranged for the metallic oxides as follows: $Ag_2O > Cu_2O > MoO_3$. This classification is found to be in agreement with literature data for oxygen atoms recombination on metallic surfaces.[32]

The freestream parameters, the enthalpy, temperature, velocity, and chemical composition at the outer edge of the boundary layer, were numerically rebuilt on the basis of the two measured parameters, the heat flux to the cooled silver surface ($T_w = 300$ K) assumed to be a fully catalytic wall and the velocity head, using multiparameter solutions of the one-dimensional boundary-layer problem for the fully catalytic wall case and an assumption of LTE in freestream.

The calculated charts of the stagnation point heat flux $q_w = q_w(T_w, \gamma_w)$ are presented in Fig. 7 for the four test regimes. The solid curves are the dependencies $q_w(T_w)$ at constant γ_w ($0 \le \gamma_w \le 1$). The upper solid curves correspond to a fully catalytic surface ($\gamma_w = 1$) and the lower curves to a noncatalytic surface ($\gamma_w = 0$). The dashed curves are the heat transfer rates for the noncatalytic surface in frozen boundary layer, that is, the lower theoretical limits of the heat fluxes.

Surface catalycity affects essentially the stagnation point heat flux in the selected test regimes. In the cold surface case ($T_w \approx 300$ K), the ratio $q_w(\gamma_w = 1)/q_w(\gamma_w = 0) \approx 1.5$–2; at high surface temperatures in the range $T_w = 1800$–2000 K this ratio approaches 4. Note that catalytic heating in the dissociated carbon dioxide flow becomes more significant at lower temperatures in freestream than in the dissociated airflows.

The contribution of the gas-phase reactions to heat transfer rates is maximal in the case of a cold noncatalytic surface (Fig. 7). With T_w increasing, the influence of the gas-phase reactions on heat transfer decreases, and heterogeneous catalysis becomes the main nonequilibrium process to influence the heat flux. Thus, all of the testing regimes performed using the IPG-4 plasmatron had close to optimal conditions for the determination of catalytic efficiency of a high-temperature quartz surface.

The measured heat fluxes to the cooled silver, copper, and molybdenum surfaces and the results of measurements of the heat flux and temperature on a quartz surface are presented in Fig. 7. All experimental data for metals and quartz are spaced within numerically designed heat flux envelopes. The data for the silver and copper are located quite close to each other. The points related to molybdenum are shifted significantly below and placed near positions that correspond to a cold noncatalytic surface. Thus, the molybdenum surface appears to be a noncatalytic one in dissociated carbon dioxide flows, as well as in dissociated air and nitrogen flows.[10,11]

In the two test regimes presented in Fig. 7a ($N_{ap} = 29$ kW, $h_e = 14$ MJ/kg, and $V_s = 43$ m/s) and in Fig. 7b ($N_{ap} = 52$ kW, $h_e = 30$ MJ/kg, and $V_s = 118$ m/s), the data for quartz are located along the curves at $\gamma_w = 0$ and 10^{-3}. In flow regimes at higher enthalpy presented in Fig. 7c ($N_{ap} = 64$ kW, $h_e = 35$ MJ/kg, and $V_s = 145$ m/s) and Fig. 7d ($N_{ap} = 72$ kW, $h_e = 39$ MJ/kg, and $V_s = 164$ m/s), the data for quartz are located quite close to the curves $\gamma_w = 3.2 \times 10^{-3}$, and one can observe some deviation of the data toward the curves $\gamma_w = 10^{-2}$ at the maximum surface temperatures. It is clear from Fig. 7 that the quartz catalytic efficiency increases with the surface temperature, increasing up to $T_w \approx 1500$ K.

Each location of the experimental point on the heat flux chart yields the only γ_w value at the measured surface temperature. Figure 8 presents the obtained γ_w data for molybdenum at $T_w = 300$ K and for quartz in the surface temperature range $T_w = 390$–1470 K according to the data shown in Fig. 7. A molybdenum surface appears as a poor catalyst at $T_w = 300$ K: The average value of $\gamma_w = 8 \times 10^{-4}$.

In the temperature range $T_w = 390$–1470 K, catalytic efficiency of quartz γ_w increases monotonously if surface temperature increases as well. There is some scattering of the data obtained at weak and moderate heat transfer regimes, but the data obtained at

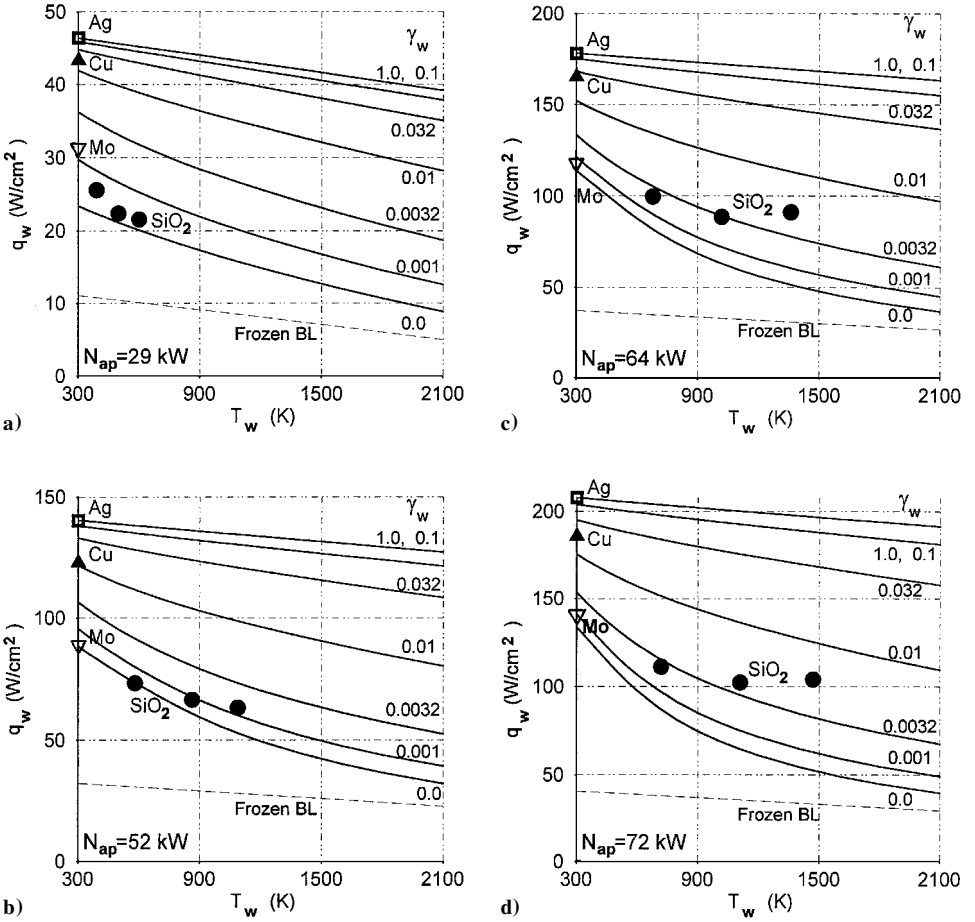

Fig. 7 Stagnation point heat fluxes to the test model in subsonic high-enthalpy CO_2 flows.

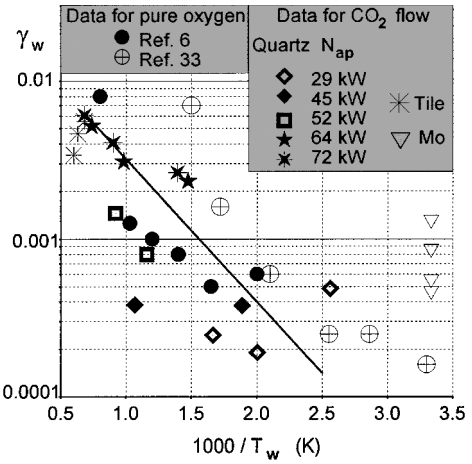

Fig. 8 Catalytic efficiencies of quartz- and silica-based surfaces in dissociated carbon dioxide mixture and pure oxygen.

strong high-enthalpy regimes showed Arrhenius-like behavior of $\gamma_w(T_w)$.

As we can see in Fig. 8, the novel data on effective quartz catalycity in dissociated carbon dioxide flows are in good agreement with the well-known data on the recombination of the oxygen atoms on quartz[33] at $T_w < 660$ K and on reaction-cured glass[6,7] applied in the space shuttle TPS in the whole studied temperature range. This finding is also consistent with the recent experimental data in Ref. 14 that O-atom recombination is the dominant surface reaction on quartz in mixtures of O and CO.

Our previous data[8] on the efficiency of the catalytic recombination of carbon monoxide and atomic oxygen on the Buran thermal-protection tile surface are also presented in Fig. 8. These data show the opposite temperature trend, but they are matched well with the present data for quartz at $T_w = 1470$ K. Taking into account the similarities of the catalytic properties of quartz and thermal-protection tile surfaces, we can combine the newly obtained data with previous data[8] collected in Fig. 8. The result reveals that the catalytic efficiency γ_w of silica-based materials reaches maximum at $T_w \approx 1470$ K in a dissociated carbon dioxide flow. Such a maximum was observed in dissociated oxygen, nitrogen, and airflows[6,7,34] as well. The existence of γ_w maximum ($\approx 6 \times 10^{-3}$) points out the change of the recombination mechanism at $T_w \approx 1470$ K: The γ_w drop with T_w increasing is a result of oxygen atoms desorption rate growth at a surface temperature above 1470 K. This result is in qualitative agreement with theoretical models already developed for atomic oxygen recombination on silica-based surfaces.[7,35,36]

Therefore, on the basis of the data in Fig. 8, we can recommend the following approximation for the catalytic efficiency of the silica-based surface in the dissociated carbon dioxide flow:

$$\gamma_w = \begin{cases} 2.58 \times 10^{-2} \exp\left(-2.08 \times 10^3 / T_w\right) \\ \qquad 390 \le T_w \le 1470 \text{ K} \\ 1.13 \times 10^{-4} \exp\left(5.79 \times 10^3 / T_w\right) \\ \qquad 1470 \le T_w \le 1670 \text{ K} \end{cases} \tag{16}$$

Note that recombination of the C atoms contributes to the heat flux at the enthalpies above 35 MJ/kg. Thus, in fact, the presented γ_w data actually correspond to the atomic oxygen and carbon monoxide recombinations.

Conclusions

Good agreement of the novel data for the average efficiency of the catalytic reactions $O + O \rightarrow O_2$ and $CO + O \rightarrow CO_2$ on a quartz surface with the well-known experimental data for oxygen atoms heterogeneous recombination points out the similarity of the recombination mechanisms on quartz surface in dissociated carbon

dioxide and pure oxygen gas flows. The Eley–Rideal mechanism, in which the adsorption of O atoms predominates over CO-molecules adsorption, is sufficient to predict the heat transfer to silica-based surfaces in dissociated carbon dioxide flows. The average catalytic efficiency γ_w follows the Arrhenius law up to surface temperature about 1470 K, with temperature increasing, quartz evaluates from a poor catalyst to a moderate one, respectively. At surface temperatures above 1470 K, the desorption of surface-adhered oxygen atoms becomes a dominant process and γ_w decreases dramatically if T_w increases. Thus, the processes of adsorption and desorption of oxygen atoms appear as the key factors in surface catalysis in dissociated carbon dioxide flows. For the applications to the Martian atmosphere entries, an approximation of $\gamma_w(T_w)$ for silica-based surfaces in the temperature range 390–1670 K is given, although it would be acceptable to use the efficiency γ_{wO} of the oxygen recombination as an upper bound for the catalytic reaction $CO + O \rightarrow CO_2$ because we can expect that $\gamma_{wCO} \leq \gamma_{wO}$ due to the steric factor. The present results, based on a simple scheme of catalysis on quartz, are generally in qualitative agreement with theoretical models already developed for atomic oxygen recombination on silica-based surfaces. Applications of such low catalytic materials in TPS for the future Mars missions look quite beneficial.

Acknowledgment

This work was supported by the International Science and Technology Center (ISTC) in Moscow (ISTC Project 036).

References

[1]Chen, Y. K., Henline, W. D., Stewart, D. A., and Candler, G. V., "Navier–Stokes Solutions with Surface Catalysis for Martian Atmospheric Entry," *Journal of Spacecraft and Rockets*, Vol. 30, No. 1, 1993, pp. 32–42.

[2]Gupta, R. N., Lee, R. N., and Scott, C. D., "Aerothermal Study of Mars Pathfinder Aeroshell," *Journal of Spacecraft and Rockets*, Vol. 33, No. 1, 1996, pp. 61–69.

[3]Kay, R. D., and Netterfield, M. P., "Thermochemical Non-Equilibrium Computations of a Mars Entry Vehicle," AIAA Paper 93-2841, July 1993.

[4]Gromov, V. G., and Afonina, N. E., "Thermochemical Nonequilibrium Computations of a Mars Express Probe," *Proceedings of the Third European Symposium on Aerothermodynamics for Space Vehicles*, edited by R. A. Harris, SP-426, ESA, 1999, pp. 179–186.

[5]Scott, C. D., "Catalytic Recombination of Nitrogen and Oxygen on High Temperature Reusable Surface Insulation," *Aerothermodynamics and Planetary Entry*, edited by A. L. Crosbie, Vol. 77, Progress in Astronautics and Aeronautics, AIAA, New York, 1981, pp. 192–212.

[6]Stewart, D. A., Henline, W. D., Kolodzeiej, P., and Pincha, M. W., "Effect of Surface Catalysis in Heating to Ceramic Coated Thermal Protection Systems for Transatmospheric Vehicles," AIAA Paper 88-2706, June 1988.

[7]Jumper, E. J., "Recombination of Oxygen and Nitrogen on Silica-based Thermal Protection Surfaces: Mechanism and Implications," *Molecular Physics and Hypersonic Flows*, edited by M. Capitelli, Vol. 482, NATO Advanced Study Inst. Series, Kluwer, Dordrecht, The Netherlands, 1996, pp. 181–191.

[8]Bykova, N. G., Vasil'evskii, S. A., Gordeev, A. N., Kolesnikov, A. F., Pershin, I. S., and Yakushin, M. I., "Determination of the Effective Probabilities of Catalytic Reactions on the Surfaces of Heat Shield Materials in Dissociated Carbon Dioxide Flows," *Fluid Dynamics*, Vol. 32, No. 6, 1997, pp. 876–886 (translated from Russian).

[9]Kolesnikov, A. F., Pershin, I. S., Vasil'evskii, S. A., and Yakushin, M. I., "Study of Quartz Surface Catalycity in Dissociated Carbon Dioxide Subsonic Flows," AIAA Paper 98-2847, June 1998.

[10]Vasil'evskii, S. A., Kolesnikov, A. F., and Yakushin, M. I., "Determination of the Effective Probabilities of the Heterogeneous Recombination of Atoms When Heat Flow Is Influenced by Gas-Phase Reactions," *High Temperature*, Vol. 29, No. 3, 1991, pp. 411–419 (translated from Russian).

[11]Kolesnikov, A. F., "The Aerothermodynamic Simulation in Sub- and Supersonic High Enthalpy Jets: Experiment and Theory," edited by J. J. Hunt, *Proceedings of the Second European Symposium on Aerothermodynamics for Space Vehicles*, SP-367, ESA, 1995, pp. 583–590.

[12]Rubio García, V., Marraffa, L., Scoon, G., Roumeas, R., and Seiler, R., "Mars Mini-Probes. Elements of Aerothermodynamics and Entry Trajectories," *Proceedings of the Third European Symposium on Aerothermodynamics for Space Vehicles*, edited by R. A. Harris, SP-426, ESA, 1999, pp. 155–162.

[13]Kolesnikov, A. F., Yakushin, M. I., Vasil'evskii, S. A., Pershin, I. S., and Gordeev, A. N., "Catalysis Heat Effects on Quartz Surfaces in High-Enthalpy Subsonic Oxygen and Carbon Dioxide Flows," *Proceedings of the Third European Symposium on Aerothermodynamics for Space Vehicles*, edited by R. A. Harris, SP-426, ESA, 1999, pp. 537–544.

[14]Sepka, S., Copeland, R., Marschall, J., and Chen, Y.-K., "Experimental Investigation of Surface Reactions in Carbon Monoxide and Oxygen Mixtures," AIAA Paper 99-3629, June 1999.

[15]Kolesnikov, A., and Marraffa, L., "An Analysis of Stagnation Point Thermochemical Simulation by Plasmatron for Mars Probe," AIAA 99-3564, June 1999.

[16]Kolesnikov, A. F., "Conditions of Simulation of Stagnation Point Heat Transfer from a High-Enthalpy Flow," *Fluid Dynamics*, Vol. 28, No. 1, 1993, pp. 131–137 (translated from Russian).

[17]Bykova, N. G., Vasil'evskii, S. A., Gordeev, A. N., Kolesnikov, A. F., Pershin, I. S., and Yakushin, M. I., "An Induction Plasmatron Application for Simulation of Entry into Martian Atmosphere," *Proceeding of the Third International Symposium on Environmental Testing for Space Programmes*, edited by T.-D. Guyenne, SP-408, ESA, 1997, pp. 195–200.

[18]Kolesnikov, A. F., Yakushin, M. I., Pershin, I. S., and Vasil'evskii, S. A., "Heat Transfer Simulation and Surface Catalycity Prediction at the Martian Atmosphere Entry Conditions," AIAA Paper 99-4892, Nov. 1999.

[19]Spirin, G. G., Vinogradov, Y. K., and Belyaev, O. V., "Experimental Study of Molecular Thermal Conductivity of Quartz," *Teplofizika Vysokih Temperatur*, Vol. 34, No. 1, 1996, pp. 29–34 (in Russian).

[20]Dvurechensky, A. V., Petrov, V. A., and Reznik, V. Y., "Experimental Study of Quartz Glass Spectral Emissivity at High Temperatures," *Teplofizika Vysokih Temperatur*, Vol. 16, No. 4, 1978, pp. 749–754 (in Russian).

[21]Petrov, V. A., and Reznik, V. Y., "Total Normal Emissivity of Quartz Glass of 'QR' Type at High Temperatures," *Teplofizika Vysokih Temperatur*, Vol. 10, No. 4, 1972, pp. 778–782 (in Russian).

[22]Vasil'evskii, S. A., Kolesnikov, A. F., and Yakushin, M. I., "Mathematical Models for Plasma and Gas Flows in Induction Plasmatrons," *Molecular Physics and Hypersonic Flows*, edited by M. Capitelli, Vol. 482, NATO Advanced Study Inst. Series, Kluwer, Dordrecht, The Netherlands, 1996, pp. 495–504.

[23]Boulos, M. I., "The Inductively Coupled Radio-Frequency Plasma," *Journal of Pure and Applied Chemistry*, Vol. 57, No. 9, 1985, pp. 1321–1352.

[24]Kolesnikov, A. F., and Vasil'evskii, S. A., "Some Problems of Numerical Simulation of Discharge Electrodynamics in Induction Plasmatron," *Computational Physics, Chemistry and Biology*, edited by A. Sydov, Vol. 3, Wissenschaft and Technik Verlag, Berlin, 1997, pp. 175–180.

[25]Patankar, S. V., *Numerical Heat Transfer and Fluid Flow*, edited by M. A. Phillips and E. M. Millman, Taylor and Francis, New York, 1980.

[26]Vanden Abeele, D., Vasil'evskii, S. A., Kolesnikov, A. F., Degrez, G., and Bottin, B., "Code-to-Code Validation of Inductive Plasma Computations," von Kármán Inst., TN-197, St. Genesius-Rode, Belgium, July 1999.

[27]Vanden Abeele, D., and Degrez, G., "An Efficient Computational Model for Inductive Plasma Flows," AIAA 98-2825, June 1998.

[28]Capitelli, M., and Devoto, R. S., "Transport Coefficients of High-Temperature Nitrogen," *Physics of Fluids*, Vol. 16, No. 11, 1973, pp. 1835–1843.

[29]Kolesnikov, A. F., and Tirskii, G. A., "Equations of Hydrodynamics for Partially Ionized Multi-Component Mixtures of Gases, Employing Higher Approximations of Transport Coefficients," *Fluid Mechanics–Soviet Research*, Vol. 13, No. 4, 1984, pp. 70–97; Scripta Technica, Washington, DC, 1985.

[30]Park, C., Howe, J. T., Jaffe, R. L., and Candler, G. V., "Review of Chemical-Kinetic Problems of Future NASA Missions, II: Mars Entries," *Journal of Thermophysics and Heat Transfer*, Vol. 8, No. 1, 1996, pp. 9–23.

[31]Hardy, W. A., and Linnett, J. W., "Mechanism of Atom Recombination on Surface," *Proceedings of 11th Symposium (International) on Combustion*, Combustion Inst., Pittsburgh, PA, 1966, pp. 167–179.

[32]Cauquot, P., Cavadias, S., and Amouroux, J., "Thermal Energy Accomodation from Oxygen Atoms Recombination on Metallic Surfaces," *Journal of Thermophysics and Heat Transfer*, Vol. 12, No. 2, 1998, pp. 206–213.

[33]Greaves, J. C., and Linnett, J. W., "Recombination of Oxygen Atoms on Silica from 20C to 600C," *Transaction of the Faraday Society*, Vol. 55, Aug. 1959, pp. 1355–1361.

[34]Stewart, D. A., Chen, Y.-K., Bamford, D. J., and Romanovsky, A. B., "Predicting Material Surface Catalytic Efficiency Using Arc-Jet Tests," AIAA Paper 95-2013, June 1995.

[35]Kovalev, V. L., Suslov, O. N., and Tirskiy, G. A., "Phenomenological Theory for Heterogeneous Recombination of Partially Dissociated Air on High Temperature Surfaces," *Molecular Physics and Hypersonic Flows*, edited by M. Capitelli, Vol. 482, NATO Aavanced Study Inst. Series, Kluwer, Dordrecht, The Netherlands, 1996, pp. 193–202.

[36]Daiß, A., Frühauf, H. H., and Messerschmid, E. W., "Chemical Reactions and Thermal Nonequilibrium on Silica Surfaces," *Molecular Physics and Hypersonic Flows*, edited by M. Capitelli, Vol. 482, NATO Aavanced Study Inst. Series, Kluwer, Dordrecht, The Netherlands, 1996, pp. 203–218.

I. D. Boyd
Associate Editor